Non-invasive 4D Blood Flow and Pressure Quantification in Central Blood Vessels via PC-MRI

Sebastian Meier[1], Anja Hennemuth[1], Ola Friman[1], Jelena Bock[2], Michael Markl[2], Tobias Preusser[1,3]

[1] Fraunhofer MEVIS, Bremen, Germany
[2] Department of Radiology, Medical Physics, University Hospital Freiburg, Germany
[3] School of Engineering and Science, Jacobs University, Bremen, Germany

Abstract

Purpose of this work is the demonstration of new methods for non-invasive assessment of detailed haemodynamical parameters in central blood vessels based on advanced postprocessing methods. In particular, we present a new finite-element-based method for computing 4D intravascular blood pressure differences. A verification using CFD methods and tests on real image data show the possible value of the method for clinical diagnosis and therapy planning.

1. Introduction

Localized blood vessel anatomy and haemodynamics play an important role for diagnosis and therapy planning in patients with arterial malformations and congenital heart diseases. Particularly, blood pressure differences along the vessel are a key factor for assessing the severity of arterial stenosis. The gold standard for determining intravascular blood pressure in clinical practice is an invasive measurement using a pressure catheter. Due to its invasive nature, this method is not applicable for screening or follow-up studies. A promising method for non-invasive determination of hemodynamical parameters is phase-contrast (or flow-sensitive) magnetic resonance imaging (PC-MRI) [1]. This method uses specially designed MRI sequences in order to encode the blood flow velocity in the phase of the measured signal. Recent progress in MRI technology has facilitated time- and spatially resolved (4D) PC-MRI providing three-directional blood flow velocities in reasonable scan times [2]. Therefore, it becomes possible to analyze not only well-established diagnostic parameters such as the mean flow rate and peak velocities but also complex flow patterns [3]. Combining the velocity information with the classical MR magnitude image, also the vessel anatomy can be determined without the use of contrast agents (so-called phase-contrast magnetic resonance angiography, PC-MRA).

It is a known fact in fluid dynamics that the relative pressure field p can be determined from the velocity field $\mathbf{v}$ by solving the Pressure Poisson equation (PPE)

$$-\Delta p = \nabla \cdot (\rho \frac{\partial}{\partial t}\mathbf{v} + \rho \mathbf{v} \cdot \nabla \mathbf{v} - \eta \nabla^2 \mathbf{v} - \rho \mathbf{g}),$$

where ρ and η are the density and dynamic viscosity of blood and $\mathbf{g}$ is the gravity force density. In [4], an iterative solution method was proposed for solving the PPE in order to non-invasively determine relative pressure fields in the human aorta based on 4D PC-MRI image data. The feasibility and accuracy of this method has been shown in subsequent papers by comparison with CFD computations [5], with catheter measurements in flow phantoms or in-vivo animal models [6] and by studies in healthy volunteers [7].

Despite of the successful evaluation studies, it has been pointed out by Ebbers & Farneback in [8] that the suggested iterative solvers of the PPE may not respect the physically correct boundary conditions and may lead to large errors for certain vessel geometries. The authors suggest a multi-grid finite-difference scheme for solving the PPE with inhomogeneous Neumann boundary conditions directly in the segmented flow volume. In the present work, we adapt this mathematical model and solve the PPE by the finite-element method (FEM) directly in the voxel grid with hexahedral elements. The advantage of this numerical scheme is twofold: First, the inhomogeneous Neumann boundary conditions can be treated much easier. Second, the symmetric system matrix allows to apply the conjugate gradient (CG) solver, which provides a simple and highly efficient numerical scheme.

2. Methods

2.1. 4D flow-sensitive MRI measurements and image processing

Phase contrast 4D MRI measurements in-vivo covering the entire thoracic aorta were performed using a respira-

tion controlled and ECG-gated RF-spoiled gradient echo sequence (velocity encoding 150 cm/s) on a 3T system at University Hospital Freiburg. The data acquisition was synchronized with the subject's ECG and respiration (spatial resolution $\sim 2\,\mathrm{mm}^3$, temporal resolution $\sim 40\,\mathrm{ms}$, total scan time 15-20 minutes) After an automatic eddy current correction and a phase unwrapping algorithm, the vessel lumen is extracted via PC-MRA calculation and watershed segmentation. This semi-automatic image processing chain is implemented in MevisLab and works also as a stand-alone software application. In addition, it allows advanced flow analysis and visualization like particle tracing and assessment of local flow rates [9].

2.2. Pressure computation

Blood flow in large arteries is usually described by the incompressible Navier-Stokes equations, which correlate the pressure in the flow domain $\Omega \subset \mathbf{R^3}$ to the three-dimensional velocity field via

$$-\nabla p = \rho \frac{\partial}{\partial t}\mathbf{v} + \rho \mathbf{v} \cdot \nabla \mathbf{v} - \eta \nabla^2 \mathbf{v} - \rho \mathbf{g} =: \mathbf{r} \quad (1)$$

The vector field $\mathbf{r}(x,t)$ can be computed from the PC-MRI data. The unknown pressure field is then subject to the minimization problem

$$\int_\Omega \|\nabla p(x,t) - \mathbf{r}(x,t)\|^2 \, dx \longrightarrow \text{min!}$$

This problem needs to be solved for each time point independently. It is uniquely solvable up to an additive constant. The equivalent variational formulation (Euler-Lagrange equation) is: Find $p = p(x,t)$ such that

$$\int_\Omega \nabla p \cdot \nabla \varphi \, dx = \int_\Omega \mathbf{r} \cdot \nabla \varphi \, dx \quad \text{for all test functions } \varphi(x)$$

For simplicity, all computations are done directly on the voxel grid by choosing eight-node hexahedral elements. The flow domain Ω is given by a binary mask. Let $\hat{V}$ be the FE space with basis functions φ_i, $i = 0, \ldots, N-1$. Note that the number of FE nodes N is *smaller* than the number of mask points, since all structures consisting of only 1 voxel in diameter are deleted from the flow domain during the assembling of the FE matrices.

Let $\mathbf{A}_{ij}$ be the stiffness matrix and $\mathbf{M}_{ij}$ the lumped (diagonal) mass matrix. In addition, the following non-symmetric matrices are needed:

$$\mathbf{L}^{(l)}_{i,j} := \int_\Omega \varphi_i \partial_{x_l} \varphi_j \, dx, \qquad l = 1, \ldots, 3$$

The procedure for computing the solution of the PPE is as follows: First, the vector quantity $\mathbf{r}$ is determined from the discrete velocity field $\mathbf{v}$ via equation (1). Here, gravity is assumed not to play a role. The time derivatives are computed via central difference quotients, while the spatial derivatives in the flow domain are computed using the FEM matrices:

$$\frac{\partial v_i}{\partial x_l} \approx \mathbf{M}^{-1} (\mathbf{L}^{(l)})^T v_i.$$

The advantage of this procedure is that no special treatment is needed in order to get the spatial derivatives at the vessel walls right, as compared to the finite-difference method. Afterwards, the flow volume is slightly reduced in order to avoid errors from the second spatial derivatives due to large noise near the vessel walls. Finally, one solves the linear system

$$\mathbf{A}\mathbf{p} = \sum_{l=1}^{3} \mathbf{L}^{(1)} \mathbf{r}^{(1)} \quad (2)$$

Since the pressure field is only determined up to an additive constant, the matrix $\mathbf{A}$ will be singular. Therefore, a Dirichlet constraint at one node is added to the problem and $\mathbf{A}$ has to be altered in the corresponding line and row. Finally, (2) is solved by the CG method. Computation times for typical image data are 2-3 seconds per time point on a standard computer.

3. Results

3.1. Verification by CFD

A stenotic vessel software phantom was constructed as shown in figure 1. Since no analytical solution exists, the reference solution is taken from a fully converged stationary CFD solution using the commercial FEM package Comsol Multiphysics. Using rotational symmetry, the CFD solution was computed on an two-dimensional unstructured tetrahedral grid of 33000 nodes and interpolated linearly to a three-dimensional voxel grid with voxel size $0.86 \times 0.86 \times 1.07\,\mathrm{mm}^3$. The vessel length was $750\,\mathrm{mm}$ and the minimal and maximal diameter were $10.3\,\mathrm{mm}$ and $33.5\,\mathrm{mm}$, respectively, which results in an effective stenosis of 90%. The dynamic viscosity of blood is estimated by $\eta = 0.00424\,\mathrm{Pa\,s}$ and the density by $\rho = 1060\,\mathrm{kg/m}^3$. The maximal flow velocity at the inlet was $v = 3\,\mathrm{cm/s}$ and therefore the inlet Reynolds number was 251. As shown in figure 1, the reconstructed pressure drop along the stenosis only slightly underestimates the CFD reference pressure drop. The relative error in the pressure field $\sum |p_i - p_i^{\mathrm{Ref}}| / \sum |p_i^{\mathrm{Ref}}|$ was 7.5%.

3.2. Application to in-vivo data

The algorithm was tested with 4D PC-MRI data from an healthy subject and from a patient with a large aneurysm

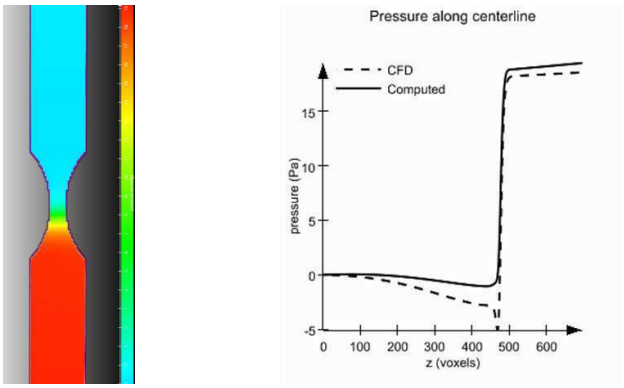

Figure 1. Reconstructed pressure field at stenosis (left) and along the centerline of the phantom vessel compared to CFD reference solution (right).

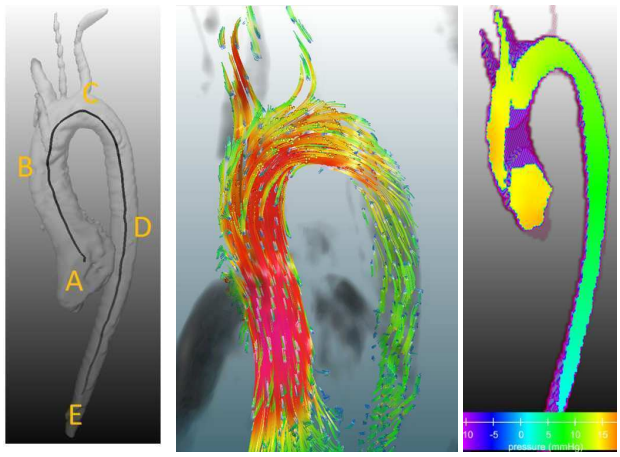

Figure 2. Geometry, streamlines and relative pressure field during systole for the healthy subject.

in the proximal descending aorta. The image resolution for the healthy subject was $48 \times 187 \times 21$ voxels at 14 time points, voxel size $1.667 \times 1.667 \times 3.5\,\mathrm{mm}^3$, time step $50\,\mathrm{ms}$. As a reference point for the pressure, the point (E) in the abdominal aorta was chosen (cf. figure 2). Since no absolute pressure measurements were available, the reference pressure was set to zero during the whole cardiac cycle, similar as done in [7]. Geometry, flow streamlines and pressure field during systole are shown in figure 2. In figure 3, pressure differences are extracted at ascending aorta (B), proximal descending aorta (C), descending aorta (D) and abdominal aorta (close to E). The value of the pressure in the left ventricle was not extracted, since it is not connected to the aortic flow domain during diastole and therefore the pressure difference may be incorrect. In figure 4, the pressure differences were plotted along the vessel centerline from points A to E. It can be seen that during diastole, the pressure drop along the aorta turns negative.

The image resolution for the aortic aneurysm case was $144 \times 192 \times 28$ voxels at 20 time points, voxel size $1.771 \times 1.771 \times 2.6\,\mathrm{mm}$, time step $40\,\mathrm{ms}$. The reference pressure was set as described above. Geometry, flow streamlines and pressure field during systole are shown in figure 5. From the flow streamlines, a vortical flow pattern in the aneurysm is clearly seen. The pressure differences over the heart cycle (figure 6) are less smooth than for the healthy subject (figure 3). The abnormality can be seen most clearly in the pressure differences along the vessel centerline (figure 7). A strong pressure drop within the aneurysm and a smaller one distal to it are observed during diastole.

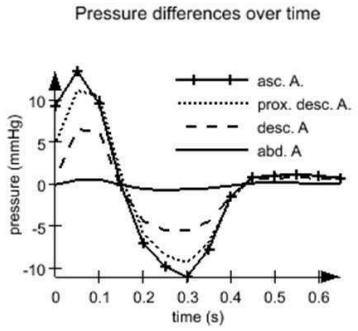

Figure 3. Pressure differences during the heart cycle for the healthy subject. Pressures are relative to point (E) (cf. figure 3).

4. Discussion and conclusions

The implementation of the Pressure-Poisson equation suggested here yields perfectly stable results in very short computation times. The CFD verification showed that the pressure drop along a severe stenosis can be predicted by our algorithm. The relative error of 7.5% is mainly attributed to interpolation errors and limited resolution. Its dependence on image resolution, noise and possible flow turbulences needs to be further investigated. The results for the healthy subject are reasonable and agree well with published data in [7]. For the aneurysm case, pressure drops along the varying vessel diameter can be clearly quantified from the computations. It is concluded that the proposed non-invasive method yields valuable information on local haemodynamic parameters and may help to improve diagnosis and therapy planning.

Acknowledgements

This work was partly funded by the European Regional Development Fund (EFRE).

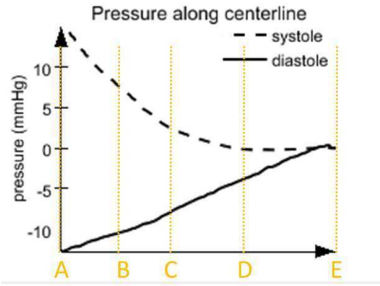

Figure 4. Pressure differences along the vessel centerline during systole and diastole for the healthy subject. Pressures are relative to point (E) (cf. figure 3).

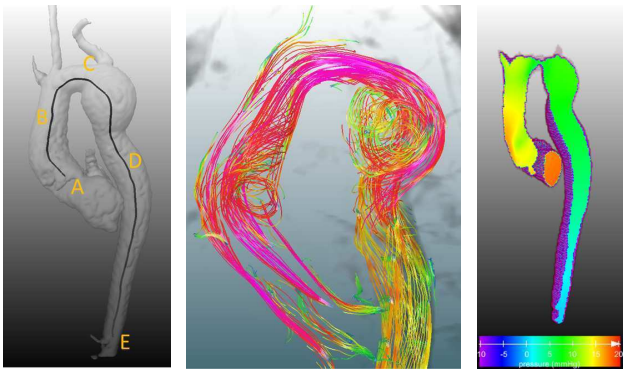

Figure 5. Geometry, streamlines and pressure during systole for the aneurysm case.

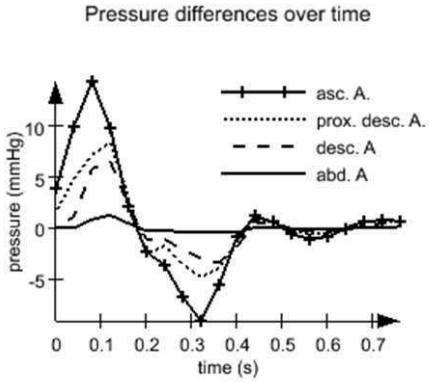

Figure 6. Pressure time curves at different positions for the aneurysm case. Pressures are relative to point (E) (cf. figure 5).

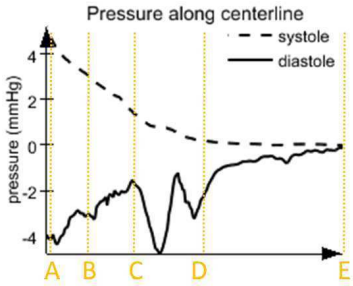

Figure 7. Pressure differences along centerline during systole and diastole for the aneurysm case. Pressures are relative to point (E) (cf. figure 5).

References

[1] Srichai M, Lim R, Wong S, Lee V. Cardiovascular applications of phase-contrast MRI. Amer J Roentgenology 2009; 192(3):662–675.

[2] Markl M, Harloff A, Bley T, Zaitsev M, Jung B, Weigang E, Langer M, Hennig J, Frydrychowicz A. Time-resolved 3D MR velocity mapping at 3T: improved navigator-gated assessment of vascular anatomy and blood flow. J Magnetic Resonance Imaging 2007;25(4):824–831.

[3] Stalder A, Russe M, Frydrychowicz A, Bock J, Hennig J, Markl M. Quantitative 2D and 3D phase contrast MRI: optimized analysis of blood flow and vessel wall parameters. Magnetic resonance in medicine 2008;60(5):1218–1231.

[4] Tyszka J, Laidlaw D, Asa J, Silverman J. Three-dimensional, time-resolved (4D) relative pressure mapping using magnetic resonance imaging. J Magnetic Resonance Imaging 2000; 12(2):321–329.

[5] Nasiraei-Moghaddam A, Behrens G, Fatouraee N, Agarwal R, Choi E, Amini A. Factors affecting the accuracy of pressure measurements in vascular stenoses from phase-contrast MRI. Magnetic Resonance in Medicine 2004;52(2):300–309.

[6] Lum D, Johnson K, Paul R, Turk A, Consigny D, Grinde J, Mistretta C, Grist T. Transstenotic pressure gradients: measurement in swine–retrospectively ECG-gated 3D phase-contrast MR angiography versus endovascular pressure-sensing guidewires. Radiology 2007;245(3):751–760.

[7] Bock J, Frydrychowicz A, Johnson KM, , Wieben O, Hennig J, Markl M. Optimized data analysis for the assessment of aortic pressure difference maps. In Proc. 17th Annual Meeting of ISMRM, Honolulu, USA, 2009; Abstract 3849.

[8] Ebbers T, Farneback G. Improving computation of cardiovascular relative pressure fields from velocity MRI. J Magnetic Resonance Imaging 2009;30(1):54–61.

[9] Hennemuth A, Bock J, Friman O, Wieben O, Markl M, Konrad O, Peitgen H. Four-dimensional Phase Contrast MR Flow Imaging: Advanced Visualization and Exploration Methods. RSNA 2009 Educational Exhibit.

Address for correspondence:

Sebastian Meier
Fraunhofer MEVIS, Universitaetsallee 29, 28359 Bremen
sebastian.meier@mevis.fraunhofer.de